Proc. of the 2018 International Symposium on Electromagnetic Compatibility (EMC Europe 2018), Amsterdam, The Netherlands, August 27–30, 2018.

Uncertainties in Rydberg Atom-based RF E-field Measurements

Matthew T. Simons, Marcus D. Kautz, Joshua A. Gordon, Christopher L. Holloway
National Institute of Standards and Technology, USA
matthew.simons@nist.gov

***Abstract*— A Rydberg atom-based electric-field measurement approach is being investigated by several groups around the world as a means to develop a new SI-traceable RF E-field standard. For this technique to be useful it is important to understand the uncertainties. In this paper, we examine and quantify the sources of uncertainty present with this Rydberg atom-based RF electric-field measurement technique.**

I. Introduction

Currently, there are limitations to existing radio frequency (RF) electric field (E-field) metrology techniques. Standard RF E-field calibrations can be known to an uncertainty of at best 5 %. E-field probes must be calibrated in a 'known' field, however, a field can only really be 'known' by measuring it with a calibrated probe, creating a chicken-and-egg dilemma. Additionally, SI-traceability paths are very long and convoluted. Rydberg atom-based electromagnetically-induced transparency (EIT) is a fundamentally different approach to RF E-field metrology [1], [2], [4], [3], [5], [6], [7], [8]. This technique is based on interactions between RF fields and atomic transitions, directly linking the RF E-field measurement to fundamental units. Through this method, the uncertainties in RF E-field metrology can be reduced below present limits. For this approach to be accepted as a standard calibration method by national metrology institutes (NMIs), a comprehensive uncertainty analysis is necessary.

Electromagnetically-induced transparency is a phenomenon in which a medium that is normally absorptive becomes transparent when exposed to a particular electromagnetic field. For example, an alkali atom vapor such as rubidium (Rb) normally absorbs a 'probe laser' with a frequency tuned to the first excited state transition. When a second 'coupling' laser is tuned to a transition from the first excited state up to a high energy level Rydberg state, a destructive quantum interference occurs and the probe laser will be transmitted through the Rb vapor. The black line in Fig. 1 shows a typical EIT peak as a function of the probe laser frequency detuning from resonance.

Because the electron is far from the nucleus, Rydberg states are very sensitive to RF fields. If an RF field that is resonant with a transition to a nearby Rydberg state is applied, the EIT transmission peak splits into two peaks (blue and red lines in Fig. 1). This is known as Autler-Townes (AT) splitting. The frequency difference Δf_0 is directly related to the strength of the applied RF E-field $|E|$ by

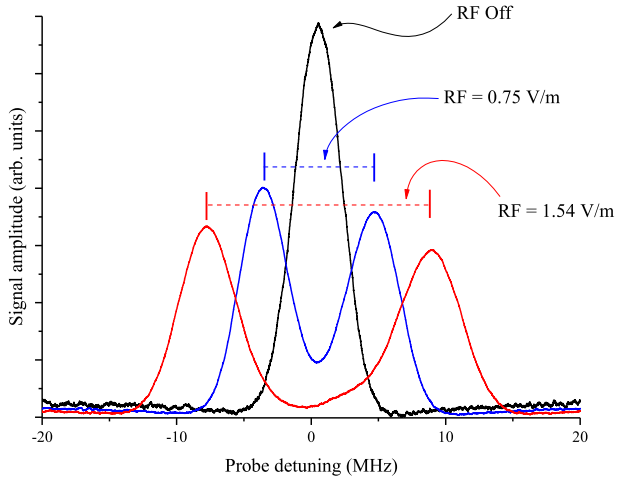

Fig. 1. EIT/AT splitting for three cases: EIT only with no RF field (black line), AT splitting with RF E-field = 0.75 V/m (blue line), AT splitting with RF E-field = 1.54 V/m (red line). The vertical axis is the transmitted probe laser intensity in arbitrary units, scaled for visibility.

$$|E| = \frac{2\pi\hbar}{\wp}\Delta f_0, \tag{1}$$

where $\hbar$ is Planck's constant and $\wp$ is the dipole moment of the transition. By calculating $\wp$ and measuring Δf_0, we directly get an SI-traceable measurement of the RF E-field strength. For example, in Fig. 1 we see that as the RF E-field is increased between the blue and red lines, the frequency separation between the peaks increases. Different frequencies can be measured by changing the frequency of the coupling laser to address different Rydberg states. Measurements can be done from ~ 0.1 GHz up to ~ 1 THz [1].

In this work we used several different glass cells evacuated and filled with a rubidium atom vapor ('vapor cells') to measure an RF field of 20.64 GHz with the Rydberg transition $47D_{5/2} \rightarrow 48P_{3/2}$. The EIT/AT signal was generated by a $\lambda_p = 780.24$ nm probe laser and a $\lambda_c = 480.270$ nm coupling laser overlapped inside the vapor cell (see Fig. 2). The laser beam diameters (full-width at half-maximum) were 270 μm, and 353 μm and the powers were 3.24 μW and 64 mW, respectively. The RF field was created by a signal generator

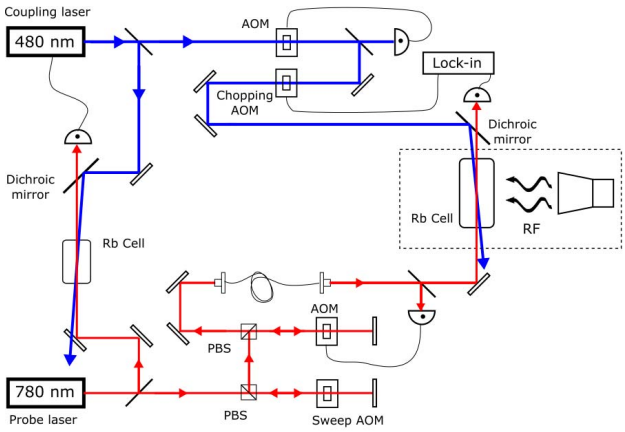

Fig. 2. Diagram of the Rydberg EIT experimental setup. The E-field measurement takes place in the area enclosed by the dashed lines. The second Rb vapor cell is used to lock the frequency of the coupling laser.

connected to a Narda 638 standard gain horn[1] placed at a distance 0.345 m from the lasers. We assessed the various sources of uncertainty through measurements of an RF field at different RF input powers and at different locations inside the vapor cell. Below we specify and quantify the uncertainties at each step in the measurement process.

II. Sources Of Uncertainty

We group the sources of uncertainty in this system into two main types, which we refer to as the 'quantum-based' uncertainties and the 'measurement-based' uncertainties. Some of these sources were examined in [2]; here we explore additional sources of uncertainty. Quantum-based uncertainties include the determination of the dipole moment $\wp$ of the Rydberg transition and the validity of the linear relationship in Eq. 1. The quantity $\wp$ must be calculated for each Rydberg transition and can be determined to within 0.1 % [9]. The conditions for linearity between $|E|$ and Δf_0 are explored in [10]. For certain experimental conditions, the uncertainty in the deviation from linearity can be kept below 0.5 %. This is determined by comparing the Rabi frequencies (measures of the intensities) of the probe laser (Ω_p), coupling laser (Ω_c), and the RF field (Ω_{RF}). The probe and coupling laser powers must be controlled such that Ω_{RF} is greater than the linewidth of the EIT peak, Γ_{EIT}, in Eq. 2. The EIT linewidth was measured to be $\Gamma_{EIT} = 2\pi \times 4.1$ MHz. The lowest RF field measured had a Rabi frequency of $\Omega_{RF} = 2\pi \times 8.6$ MHz, just over twice the EIT linewidth,

$$\Omega_{RF} > 2 \times \Gamma_{EIT}. \tag{2}$$

The measurement uncertainties are divided into three categories: (1) frequency scaling, (2) repeatability/peak measurement, and (3) vapor cell parameters. In the following sections we quantify the contributions of each of these to the overall measurement uncertainty budget for Rydberg atom-based RF E-field measurements.

[1]Certain commercial equipment, instruments, or materials are identified in this paper in order to specify the experimental procedure adequately. Such identification is not intended to imply recommendation or endorsement by the National Institute of Standards and Technology, nor is it intended to imply that the materials or equipment identified are necessarily the best available for the purpose.

III. Frequency Scaling

In order to measure the frequency difference between the AT peaks, the frequency scale (the x-axis in Fig. 1) must be calibrated. The frequency difference between the AT split peaks Δf_0 is related to the measured splitting Δf_m by $\Delta f_0 = D_\lambda \Delta f_m$. The factor $D_\lambda = \lambda_p/\lambda_c$ when the probe laser frequency is scanned and $D_\lambda = 1$ when the coupling laser frequency is scanned (see [10]). For the measurements discussed in this work, we scanned the probe laser using a voltage controlled oscillator (VCO)-driven acousto-optic modulator (AOM). The VCO was controlled with a 5 Hz, 2 V peak-to-peak triangle wave out of a high-voltage amplifier fed by a function generator. The VCO converted the input voltage to an RF signal at 10.37 MHz/V ± 0.05 MHz/V. We measured the peak-to-peak of the triangle wave with an oscilloscope, which for these measurements was $V_{pp} = 2.10$ V ± 0.14 V. The frequency was measured to be 5 Hz to 10 ppm. Combined, this translates to an uncertainty of 6.8 % in the measured frequencies.

There are ways to improve the frequency scale calibration. The main limitation above is in the scope used to measure the voltage fed to the VCO. Using a better scope can significantly reduce the uncertainty, down to below 1.8 %. The best method is to use two known atomic lines to calibrate the scale. For instance, the hyperfine transition lines in Rb are known to 0.06 %. Since we are detuning the probe around the $|5S_{1/2}, F = 3\rangle$ to $|5P_{3/2}, F' = 4\rangle$ transition, we can use the frequency difference between this and the $|5S_{1/2}, F = 3\rangle$ to $|5P_{3/2}, F' = 3\rangle$ transition, which is 120.640$\pm$0.068 MHz [11]. Combining this with the scope timescale uncertainty results in an uncertainty in our frequency scale of 0.06 %. We have not yet implemented this into our system as our AOM scan is only over 40 MHz.

IV. Repeatability

The AT splitting was determined by fitting the signal and finding the peak locations. The AT signal is most similar to a double Gaussian, but is actually a more complicated function. Figure 3 shows an example of peak fitting. The black dots are the raw data, the blue dashed line is a double Gaussian fit to the data, and the red solid line is a smoothing spline. In the inset, the double Gaussian fit is off from the actual peak by $\sim$ 0.5 MHz. For a splitting of 10 MHz, this is an error of 5 %. To better fit the data, it was smoothed with a smoothing spline, and the split was measured by finding the location of the maximum of each peak.

Four runs of data were collected as the RF power input to the horn antenna was varied. Each data run contained 10 data points at each of 17 different powers. These 10 points were then averaged and the standard deviation calculated. The averaged data are shown in Figure 4. To assess the uncertainty

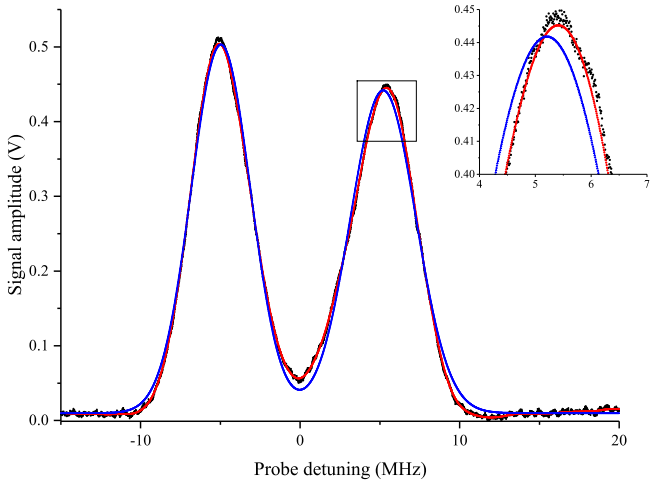

Fig. 3. Sample splitting measurement (black dots) with double Gaussian fit (blue dashed line) and smoothing spline (red solid line).

from the peak fitting, we looked at the standard deviations of the averaged points. Between all four runs the average standard deviation was less than 0.5 %. This compares to the statistical uncertainty in [2].

V. Vapor Cell Parameters

While the atoms are measuring the absolute strength of the RF E-field that they observe, that E-field strength differs from the strength outside of the vapor cell due to the properties of the dielectric cell. There are two main factors that affect the apparent E-field strength: the dielectric constant of the glass and the shape/size of the vapor cell. These are manifested in two dominant effects. First, the E-field strength is reduced as the RF field enters the vapor cell, both from dielectric loss and reflection. The dielectric loss from the vapor cell material depends on the frequency of the E-field. Second, the dielectric vapor cell acts as a cavity, forming a standing wave in the

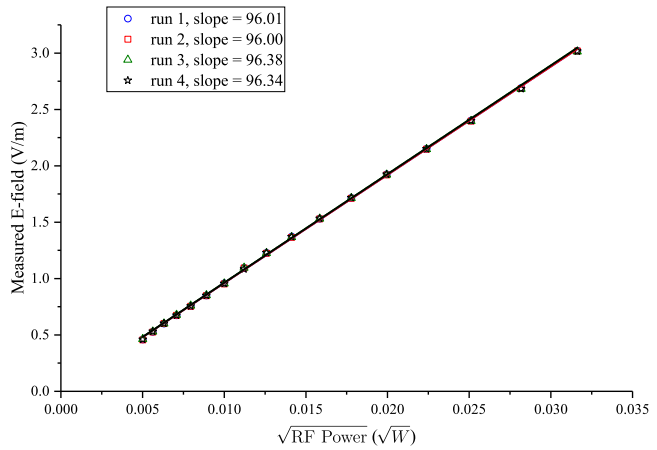

Fig. 4. Measured RF E-field vs. RF power input to horn for four separate runs.

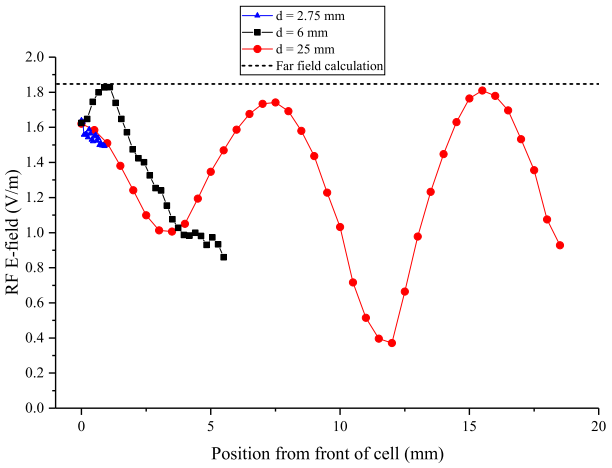

Fig. 5. Measured RF E-field vs. laser position inside cell for three different vapor cells.

E-field [12], [13]. Figure 5 shows the measured E-field strength as the lasers were scanned across three vapor cells (in the direction of the RF field propagation).

The three vapor cells used were all cylindrical glass cells, 75 mm long (along direction of laser field propagation), and had inside diameters of $d = 2.75$ mm, 6 mm, and 25 mm. An RF field with frequency 20.64 GHz and input-to-horn power of -7.9 dBm was applied with a Narda 638 standard gain horn[1] (gain of 15.9 dB) at a distance of 0.345 mm from the overlapped lasers. A far-field calculation of the E-field based on the horn gain and distance is also shown in Fig. 5. If there is no knowledge about the location of the lasers inside the vapor cell, the uncertainty in the measured field can be very large. The standing wave scales with the ratio of RF wavelength to cell diameter (λ_{RF}/d), so if the diameter is sufficiently small compared to the wavelength the field variation can be made small. For instance, the $d = 25$ mm cell has a $\lambda_{RF}/d = 0.58$, and the field varies by more than 55 % across the diameter of the cell. Using a cell with a $\lambda_{RF}/d = 7.2$ ($d = 2.75$ mm), the variation can be reduced to ~ 5 %. For a cell $\lambda_{RF}/d > 20$, the variation due to the standing wave is effectively eliminated. However, this is difficult to achieve for high frequencies (for 20.64 GHz the cell would have to be less than 1 mm).

Another way to account for this is to simulate the standing wave pattern to predict the correction factor. Figure 6 shows an example of HFSS simulations[1] compared to measured E-field data from different vapor cells [3]. As the size of the beam is less than 0.5 mm, the variation of the field within this range at a standing wave peak is 0.5 %. Using these simulations, and by measuring the location of the beam inside the vapor cell, the uncertainty associated with the field variation in the cell can be reduced to below ~ 1 %, even for a small λ_{RF}/d ratio. If the beam is located at a standing wave peak, the uncertainty is on the order of 0.5 %.

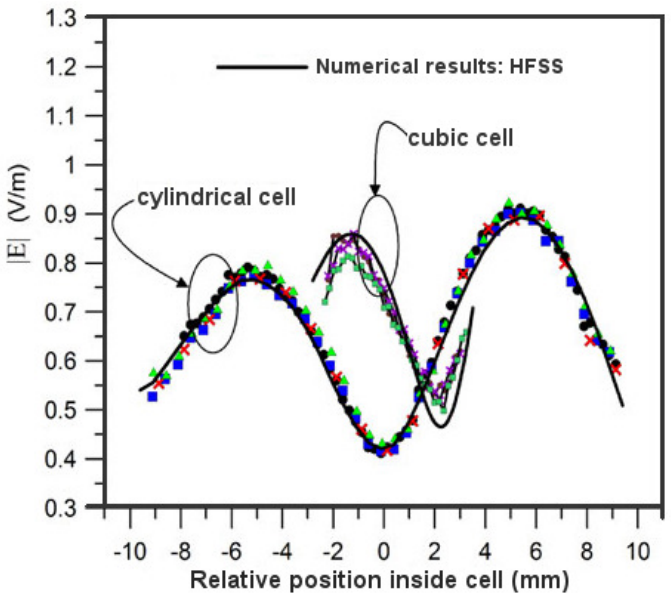

Fig. 6. Example of HFSS simulation comparison to cell position data, from [3]. Data are from multiple runs on both a cylindrical vapor cell and a cubic vapor cell.

VI. Uncertainty Budget

For an estimate of the overall uncertainties, we collected the measurement uncertainties as determined above, including the frequency scale, peak finding, and vapor cell location. We also took into account the quantum-based uncertainties as determined in previous work, for the dipole moment calculation and the deviation from linearity. An initial uncertainty budget is presented in Table 1. These values assume ideal measurement conditions, such as the beam position within the vapor cell is known, the RF E-field Rabi frequencies are greater than the EIT linewidth, and the frequency scale is calibrated to an atomic transition.

Table 1. **Uncertainty Budget**

Source		Uncertainty
Frequency Scale	δf_s	0.06 %
Peak Finding	δf_i	0.5 %
Vapor Cell Location	δE_v	1.0 %
Deviation from Linearity	δE_l	0.5 %
Dipole Moment	$\delta\wp$	0.1 %
Total	$\delta\|E\|$	< 1.4 %

The uncertainty from the frequency scale (δf_s) is small enough that it does not significantly affect the combined uncertainty. The uncertainty in the measured frequency separation (δf_m) is then determined by combining the uncertainties from the measurement of each peak location (δf_i) in Eq. 3. The uncertainty in the measurement of the E-field (δE_m) is determined using Eq. 1, by adding the uncertainty from the dipole moment calculation, $\delta\wp$, in Eq. 4. Lastly, the E-field measurement uncertainty is combined with uncertainty from the vapor cell location (δE_v) and deviation from linearity δE_l), in Eq. 5. The resulting combined uncertainty is less than 1.4 %

$$\delta\Delta f_m = \sqrt{\delta f_1^2 + \delta f_2^2} = 0.71\ \%, \quad (3)$$

$$\delta E_m = |E_m| \times \sqrt{\left(\frac{\delta\Delta f_m}{\Delta f_m}\right)^2 + \left(\frac{\delta\wp}{\wp}\right)^2} = 0.73\ \%, \quad (4)$$

$$\delta|E| = \sqrt{\delta E_m^2 + \delta E_v^2 + \delta E_l^2} = 1.34\ \%. \quad (5)$$

VII. Conclusions

The sources of uncertainty in Rydberg EIT-based RF E-field measurements must be understood for this technique to be useful as a calibration standard. The quantum-based uncertainties, from the dipole moment calculation and the deviation from linearity, have been previously determined [9], [10]. The measurement uncertainties in Rydberg EIT-based RF E-field measurements are from three main sources: the frequency scale, peak fitting, and the vapor cell parameters. The quantum based uncertainties can be limited by ensuring the experimental parameters are in the linear regime. The frequency scale and peak fitting uncertainties can likewise be controlled. The most difficult source to work with is the RF standing wave, and this uncertainty can be limited by measuring the vapor cell location and modeling the field distribution. Taking these steps, the uncertainties in this technique can be reduced to below those in present standard calibrations.

Acknowledgment

The authors thank Amanda Koepke at NIST for assistance with statistical uncertainties.

References

[1] C.L. Holloway, J.A. Gordon, A. Schwarzkopf, D.A. Anderson, S.A. Miller, N. Thaicharoen, and G. Raithel, "Broadband Rydberg Atom-Based Electric-Field Probe for SI-Traceable, Self-Calibrated Measurements", *IEEE Trans. on Antenna and Propag.*, **62**(12), 6169-6182, 2014.

[2] J. Sedlacek, A. Schwettmann, H. Kübler, R. Löw, T. Pfau, and J.P Shaffer, "Microwave electrometry with Rydberg atoms in a vapour cell using bright atomic resonances", *Nature Physics*, **8**, 819, 2012.

[3] C.L. Holloway, M.T. Simons, J.A. Gordon, P.F. Wilson, C.M. Cooke, D.A. Anderson, and G. Raithel, "Atom-Based RF Electric Field Metrology: From Self-Calibrated Measurements to Subwavelength and Near-Field Imaging", *IEEE Trans. on Electromagnetic Compat.*, **59**(2), 717-728, 2017.

[4] J.A. Sedlacek, A. Schwettmann, H. Kübler, and J.P. Shaffer, "Atom-Based Vector Microwave Electrometry Using Rubidium Rydberg Atoms in a Vapor Cell", *Phys. Rev. Lett.*, **111**, 063001, 2013.

[5] H. Fan, S. Kumar, J. Sedlacek, H. Kübler, S. Karimkashi and J.P Shaffer, "Atom based RF electric field sensing", *J. Phys. B: At. Mol. Opt. Phys.*, **48**, 202001, 2015.

[6] M. Tanasittikosol, J.D. Pritchard, D. Maxwell, A. Gauguet, K.J. Weatherill, R.M. Potvliege and C.S. Adams, "Microwave dressing of Rydberg dark states", *J. Phys B*, **44**, 184020, 2011.

[7] C.G. Wade, N. Sibalic, N.R. de Melo, J.M. Kondo, C.S. Adams, and K.J. Weatherill, "Real-time near-field terahertz imaging with atomic optical fluorescence", *Nature Photonics,* **11**, 40-43, 2017.

[8] D.A. Anderson, S.A. Miller, G. Raithel, J.A. Gordon, M.L. Butler, and C.L. Holloway, "Optical Measurements of Strong Microwave Fields with Rydberg Atoms in a Vapor Cell", *Physical Review Applied*, **5**, 034003, 2016.

[9] M.T. Simons, J.A. Gordon,C.L. Holloway, "Simultaneous use of Cs and Rb Rydberg atoms for dipole moment assessment and RF electric field measurements via electromagnetically induced transparency", *Journal of Applied Physics*, **120**, 123103, 2016.

[10] C.L. Holloway, M.T. Simons, J.A. Gordon, A. Dienstfrey, D.A. Anderson, and G. Raithel, "Electric field metrology for SI traceability: Systematic measurement uncertainties in electromagnetically induced transparency in atomic vapor", *J. of Applied Physics*, **121**, 233106-1-9, 2017.

[11] D. A. Steck, *Rubidium 85 D Line Data, available online at http://steck.us/alkalidata*, revision 2.1.6, 20 September 2013.

[12] C.L. Holloway, J.A. Gordon, A. Schwarzkopf, D.A. Anderson, S.A. Miller, N. Thaicharoen, and G. Raithel, "Sub-wavelength imaging and field mapping via electromagnetically induced transparency and Autler-Townes splitting in Rydberg atoms", *Applied Physics Letters*, **104**, 244102, 2014.

[13] H. Fan, S. Kumar, J. Sheng, J.P. Shaffer, C.L. Holloway and J.A. Gordon, "Effect of Vapor-Cell Geometry on Rydberg-Atom-Based Measurements of Radio-Frequency Electric Fields", *Physical Review Applied*, **4**, 044015, Nov., 2015.